A Nonlinear Coordinated Approach to Enhance the Transient Stability of Wind Energy-Based Power Systems

Mohammad Javad Morshed, *Member, IEEE*

***Abstract*—This paper proposes a novel framework that enables the simultaneous coordination of the controllers of doubly fed induction generators (DFIGs) and synchronous generators (SGs). The proposed coordination approach is based on the zero dynamics method aims at enhancing the transient stability of multi-machine power systems under a wide range of operating conditions. The proposed approach was implemented to the IEEE 39-bus power systems. Transient stability margin measured in terms of critical clearing time along with eigenvalue analysis and time domain simulations were considered in the performance assessment. The obtained results were also compared to those achieved using a conventional power system stabilizer/power oscillation (PSS/POD) technique and the interconnection and damping assignment passivity-based controller (IDA-PBC). The performance analysis confirmed the ability of the proposed approach to enhance damping and improve system's transient stability margin under a wide range of operating conditions.**

***Index Terms*—Doubly fed induction generator (DFIG), excitation controller, multi-machine power system, synchronous generator (SG), transient stability, zero dynamics.**

I. Introduction

TRANSIENT stability is one of the most challenging problems in large scale power systems [1]. It refers to the power system's ability to converge to a stable post-fault equilibrium following large disturbances such as faults, overload, or loss of generating units. Random oscillations caused by faults, sudden changes in loads, lightning may lead to transient instability and subsequently voltage collapse and blackouts. The increased penetration of wind energy systems into the grid have led to additional challenges to power system's stability. This is mainly due to the intermittent power availability of DFIG-based wind turbines along with the differences in the dynamic behavior characteristics of their generators compared with the conventional synchronous generators (SGs) [1]–[4]. Power system stabilizers (PSSs) have traditionally been considered to enhance both the transient and dynamic stability of SGs [5], while DFIGs were equipped with power oscillation damping (POD) devices to effectively damp power system oscillations [6], [7]. However, because the operating points of power systems change remarkably, linear approaches such as PODs and PSSs lack the necessary robustness under all operating conditions. Further, system nonlinearities can also affect power system characteristics during large disturbances, hence limiting the damping properties of PODs/PSSs. Finally, the interactions between the conventional SGs and DFIGs, which are widely deployed in wind energy systems, may cause dynamic instability in the absence of coordinated control designs. Hence, it is imperative to coordinate the design of the various controllers of the DFIGs and SGs while also taking into consideration power system's nonlinearities in wind energy-based power systems [8], [9].

Nonlinear excitation controllers were recently proposed to overcome the limitations of linear techniques and enhance the transient stability of large scale power systems in a much better way than the conventional techniques. A control structure based on two switching controllers working in a coordinated manner was proposed in [10] to enhance the transient stability of multi-machine power systems. A decentralized adaptive excitation control scheme was proposed in [11] for a three-machine power system. It was shown to enhance transient stability in the event of a large sudden fault. A decentralized multivariable adaptive voltage and speed regulator was proposed in [12] to stabilize power systems with multiple SGs. The approach was based on a nonlinear linearizing part with time varying parameters and an auxiliary stabilizing one and was shown to improve system stability and transient performance when implemented to a four-machine power system. An exact feedback linearizing excitation controller was proposed in to improve the stability margin of power systems under various operating conditions [13]. However, the implementation of exact feedback linearizing excitation controllers requires using an observer for rotor angle estimation [14]. A nonlinear approach based on the interconnection and damping assignment passivity-based control (IDA-PBC) was proposed in [15]. The IDA-PBC control design methodology was used to achieve power angle stability and provide both frequency and voltage regulation for DFIGs, SGs, and STATCOM. Success of the IDA-PBC design, however, relied on the suitable selection of the closed-loop interconnection structure and dissipation matrices and no general method currently exists for their selection, thus making its implementation to large scale power systems quite

Manuscript received February 29, 2020; accepted April 13, 2020. Recommended by Associate Editor Qinglai Wei.

Citation: M. J. Morshed, "A nonlinear coordinated approach to enhance the transient stability of wind energy-based power systems," *IEEE/CAA J. Autom. Sinica*, vol. 7, no. 4, pp. 1087–1097, Jul. 2020.

M. J. Morshed is with the Department of Electrical and Computer Engineering, University of Louisiana at Lafayette, Lafayette, LA 70504 USA (e-mail: morshed@louisiana.edu).

Color versions of one or more of the figures in this paper are available online at http://ieeexplore.ieee.org.

Digital Object Identifier 10.1109/JAS.2020.1003255

challenging [15].

Partial feedback linearization, or zero dynamics (ZD), approach have recently been considered to design excitation controllers for synchronous generators in multi-machine power systems [16]. In [17] the approach was used to allow the decoupling of the multi-machine power system based on the excitation control inputs of the synchronous generators. Among the attractive features of the zero dynamics (ZD) approach are its ability to 1) convert system's highly nonlinear dynamics into a partial linear one algebraically; 2) lead to a transformed system that is of reduced order and independent of the operating point. Further, ZD does not require the full model dynamics of the system [18].

This paper focuses on the design of a coordinated approach based on the ZD technique for large scale power systems. The proposed approach takes into consideration the various interactions between SGs and DFIGs along with system nonlinearities. It aims at enhancing the transient stability of large scale power systems with DFIG-based wind energy systems. The main features of the proposed approach are, its ability to:

1) A framework that enables the simultaneous coordination between SGs and DFIGs controllers. Contrary to existing approaches which either coordinate the design between SGs only [19], [20], or DFIGs only [21]. Further, the proposed methodology was developed for large scale power systems with *m*-SGs and *n*-DFIGs, making it easily implemented to large scale complex power systems, which is one of the most significant contributions of this manuscript.

2) A design methodology that takes into consideration the interactions between the SGs and DFIGs in multi-machine power systems. Contrary to existing approaches which omitted those interactions and resulted in poor dynamic stability [7], [19]–[23].

3) A coordinated design to handle system nonlinearities, uncertainties and the differences in the dynamic behavior of all the generators. Existing approaches [19], [20], [24]–[26] have either considered an exact linearization or a traditional zero dynamics approach.

The remainder of the paper is organized as follows. The dynamic models of the synchronous generators (SGs) and DFIGs are described in Section II. The proposed coordinated design is detailed in Section III. The performance of the proposed approach is illustrated in Section IV. A comparison analysis with other control approaches is also reported in that section. Some concluding remarks are finally given in Section V.

II. Power System's Modelling

Consider a multi-machine power system with *m*-SGs and *n*-DFIG-based wind energy systems. The dynamic models of each SG and DFIG can be represented as follows.

A. Synchronous Generator (SG) Model

The precise model of SGs is exceedingly complex and simplifications are often used in the modelling to enable any control design [27]. In our approach, we have considered a classical third-order synchronous generator model. This was motivated by the fact that this model is the most reliable in capturing the dynamics of synchronous generators when dynamic excitation needs to be taken into account [28]. The nonlinear dynamic model of the i-th SG for $i = 1,\ldots,m$ can be represented as follows [29]:

$$\begin{cases} \dot{\delta}_i = \omega_i - \omega_s \\ \dot{\omega}_i = -\dfrac{D_i}{2H_i}(\omega_i - \omega_s) - \dfrac{\omega_s}{2H_i}(P_{Ei} - P_{Mi}) \\ \dot{E}'_{qi} = \dfrac{1}{T'_{di0}}\left(E_{fdi} - E'_{qi} - \left(x_{di} - x'_{di}\right)I_{di}\right) \end{cases} \tag{1}$$

where, δ_i, ω_i, ω_s are the rotor angle, rotor speed, and rotor synchronous speed of the i-th SG, respectively. D_i, H_i, P_{Ei}, and P_{Mi} are the damping coefficient, moment of inertia, electrical power, and mechanical power of the i-th SG, respectively. E'_{qi}, E_{fdi}, T'_{Gdi0}, I_{Gdi}, x_{di}, and x'_{di} are the q-axis component of the transient internal electro-motive force, d-axis component of the field voltage, open circuit transient time constant, d-axis component of the generator's current, d-axis component of the generator's transient reactance, and d-axis component of the steady-state transient reactance of i-th SG, respectively. The precise model of synchronous generators is exceedingly complex and simplifications are often used in the modelling so as to enable any control design. In the dynamic analysis of any practical power system, when we take into account the dynamic excitation, the most reliable model is the third-order model. Because it possesses simplicity and calculation of dynamic states, it is widely used in the dynamic analysis of power systems, which does not require very high precision. In addition, the third-order model can be enough to complete the simulation study to power system simulation. Hence, the third-order model can be enough to complete the simulation study to power system simulation.

B. Doubly Fed Induction Generator (DFIG) Model

The dynamic model of the k-th DFIG for $k = 1,\ldots,n$ can be represented as follows [28]:

$$\begin{cases} \dot{D}_k = W_k - \dfrac{x_k - x'_k}{T'_{k0}x'_k}\dfrac{V_k \sin(D_k - \theta_k)}{e'_k} + \dfrac{a_{1k}V_{rk}}{e'_k} \\ \dot{W}_k = -\dfrac{D_k}{2H_k}(W_k - W_s) - \dfrac{1}{2H_k}(P_{ek} - P_{mk}) \\ \dot{e}'_k = -\dfrac{x_k}{T'_{k0}x'_k}e'_k + \dfrac{x_k - x'_k}{T'_{k0}x'_k}V_k \cos(D_k - \theta_k) + a_{2k}V_{rk} \end{cases} \tag{2}$$

where, D_k, W_k, W_s are the rotor angle, rotor speed, and rotor synchronous speed of the k-th DFIG, respectively. x_k and x'_k are the d-axis component of the generator's transient reactance and d-axis component of the steady-state transient reactance of the i-th DFIG, respectively. D_k and H_k are the damping coefficient and moment of inertia of the k-th DFIG, respectively. The parameters a_1 and a_2 are $a_1 = W_s\cos(D_k - \theta_{rk})$ and $a_2 = W_s\sin(D_k - \theta_{rk})$, respectively. V_k, e'_k, and T'_{k0} are the stator terminal voltage, internal voltage behind transient reactance $\left(x'_k\right)$, and rotor circuit constant of the k-th DFIG, respectively. V_k and θ_k are the magnitude and angle of terminal voltage of the i-th DFIG, respectively. V_{rk} and θ_{rk} are the magnitude and angle of rotor voltage of the i-th DFIG, respectively. H_k, P_{ek}, and P_{mk} are the damping coefficient, moment of inertia, electrical power, and mechanical power of

the k-th DFIG, respectively.

For the DFIG dynamics, we have adopted the dynamic model proposed by Elkington [30]. Although this DFIG model is analogous [31] to a one axis model of a synchronous machine, there are significant differences, i) e'_k is analogous to a voltage behind a transient reactance in a synchronous generator despite the fact that it is not generated from an external excitation current; ii) the angle D_k is similar to the angle of the rotor flux magnitude with respect to the synchronously rotating reference frame not a stroboscopic angle of rotation of the shaft; and iii) the angle dynamics in the first equation of (2) contains two extra terms as compared with the angle equation of a synchronous machine because of the variable speed operation of the DFIG. Replacing the second and third terms of the angle equation with $-S_k W_s$ $\left(-S_k W_s = \dfrac{x_{dk}-x'_{dk}}{T'_{dk0}x'_{dk}}\dfrac{V_k \sin(D_k-\theta_k)}{e'_k}+\dfrac{a_{1k}V_{rk}}{e'_k}\right)$, results in $\dot{D}_k = W_k - S_k W_s$. Note that S_k is the rotor slip of the i-th DFIG.

C. Active Power of SGs and DFIGs

Generally, the active power of the n-th machine in multi-machine power system with m machine can be calculated by $P_{Ei} = E'_{qi} I_{qi}$. In this power system, the I_{qi} is calculated based on the Thevenin model of the power system as $I_{qi} = E'_{qi} \times \sum_{j=1\ j\neq i}^{m}$. It is worth to note that the conductance of the transmission lines is neglected. Therefore, the active power of each machine in multi-machine can be calculated based on these calculations, and the formula can be extended for multi-machine power system with m synchronous machine and n DFIG based wind turbines.

The output electrical power of the k-th SG (P_{Ei}) can be expressed as follows:

$$P_{Ei} = E'_{qi}\sum_{\substack{j=1\\ j\neq i}}^{m} E'_{qj}\, B_{ij}\sin\delta_{ij} + E'_{qi}\sum_{j=m+1}^{m+n} e'_j\, B_{ij}\sin\left(\delta_i - D_j\right). \quad (3)$$

The output electrical power of the k-th DFIG (P_{ek}) can be expressed as follows:

$$P_{ek} = e'_k\sum_{j=1}^{m} E'_{qj}\, B_{kj}\sin\left(D_k-\delta_j\right) + e'_k\sum_{\substack{j=m+1\\ j\neq k}}^{m+n} e'_j\, B_{kj}\sin D_{ij} \quad (4)$$

where, B_{ij} is the (i, j) element of the admittance matrix of the power system.

III. Zero Dynamics Technique

First order approximation of system's dynamics around a given operating point is conventionally considered in linearizing nonlinear systems. While this technique yields satisfactory performance for systems with slowly varying equilibrium, it is not suitable for systems with inherently nonlinear dynamics [32] since it neglects high-order dynamics. Zero dynamics approach is a technique that transforms a nonlinear system to a linear one so that linear control methodologies can be used. Unlike conventional linearization, zero dynamics yields an input-output linear behavior that is valid globally, rather than in the vicinity of an equilibrium point [32]–[34].

Consider the following state space model for the nonlinear multi-machine power system:

$$\begin{cases}\dot{x}(t) = f(x) + g(x)u\\ y(t) = h(x)\end{cases} \quad (5)$$

where the state vector is represented by $x \in \mathbb{R}^N$; the control vector by $u \in \mathbb{R}^M$ and the output vector by $y \in \mathbb{R}^N$. $f(x)$ is an N-dimensional vector field in the state-space, with $N = 3(m+n)$, and $g(x)$ an M-dimensional vector with M representing the number of control inputs.

By defining, $\Delta P_E = P_E - P_M$, $\Delta P_e = P_e - P_m$, $\Delta\omega = \omega - \omega_s$, $\Delta\delta = \delta - \delta_0$,where is δ_0 the pre-fault steady state of rotor angle and $\Delta W = W - W_s$, we can re-write the dynamic model of the overall power system as follows:

$$\begin{cases}\Delta\dot{\delta}_i = \Delta\omega_i\\ \Delta\dot{\omega}_i = -\dfrac{D_i}{2H_i}\Delta\omega_i - \dfrac{\omega_s}{2H_i}\Delta P_{Ei}\\ \dot{E}'_{qi} = \underbrace{-\dfrac{1}{T'_{di0}}\left(E'_{qi} + \left(x_{di}-x'_{di}\right)I_{di}\right)}_{\tilde{f}_{1i}} + \dfrac{u_i}{T'_{di0}}, \quad i = 1,2,\ldots,m\\ \dot{D}_k = \underbrace{W_k - \dfrac{x_k - x'_k}{T'_{k0}x'_k}\dfrac{V_k\sin(D_k-\theta_k)}{e'_k}}_{\tilde{g}_{1k}} + \dfrac{a_{1k}u_{Dk}}{e'_k}\\ \Delta\dot{W}_k = -\dfrac{D_k}{2H_k}\Delta W_k - \dfrac{W_s}{2H_k}\Delta P_{ek}, \quad k = 1,\ldots,n\\ \dot{e}'_k = \underbrace{-\dfrac{x'_k}{T'_{k0}x'_k}e'_i + \dfrac{x_k - x'_k}{T'_{k0}x'_k}V_k\cos(D_k-\theta_k)}_{\tilde{g}_{2i}} + a_{2k}u_{Dk}\end{cases} \quad (6)$$

where, u_i and u_{Dk} are the input variables of the i-th SG and k-th DFIG which are equal to E_{fdi} and V_{rk}, respectively. Note that δ_i is estimated using the approach proposed in [35], while D_k and θ_{rk} are estimated by the approach outlined in [19]. For each SG and DFIG, the active powers defined by $\Delta P_E = P_E - P_M$ and $\Delta P_e = P_e - P_m$, respectively are considered as output functions.

System (6) can be represented using the Nth order ($N = n + m$) state space model (5), with $f(x)$, $g(x)$, and u defined by (7), and the output $h = [h_1 \ \ldots\ h_m\ h_{m+1}\ \ldots\ h_{m+n}]^T$ is equal to $[\Delta P_{E1}\ \ldots\ \Delta P_{Em}\ \Delta P_{e1}\ \ldots\ \Delta P_{en}]^T$.

The proposed methodology has been developed for large scale power systems with m-SGs and n-DFIGs, making it easily implemented to large scale complex power systems, which is one of the most significant contributions of this manuscript. According to (5), the state space model for the nonlinear multi-machine power system has been calculated to design the proposed controller, so we just calculated the functions $f(x)$, $g(x)$, $h(x)$ and u. It is worth to note that with m SGs and n DFIGs in the coordination procedure. Therefore, the dimension of the $\dot{x}(t)$, $f(x)$, $g(x)$, $h(x)$, and u are $3(m+n)\times 1$, $3(m+n)\times 1$, $3(m+n)\times 3(m+n)$, $1\times 3(m+n)$, $3(m+n)\times 1$.

$$\begin{bmatrix} \dot{x}_{11} \\ \dot{x}_{21} \\ \dot{x}_{31} \\ \vdots \\ \dot{x}_{1m} \\ \dot{x}_{2m} \\ \dot{x}_{3m} \\ \dot{x}_{1(m+1)} \\ \dot{x}_{2(m+1)} \\ \dot{x}_{3(m+1)} \\ \vdots \\ \dot{x}_{1(m+n)} \\ \dot{x}_{2(m+n)} \\ \dot{x}_{3(m+n)} \end{bmatrix} = \begin{bmatrix} \Delta\dot{\delta}_1 \\ \Delta\dot{\omega}_1 \\ \dot{E}'_{q1} \\ \vdots \\ \Delta\dot{\delta}_m \\ \Delta\dot{\omega}_m \\ \dot{E}'_{qm} \\ \dot{D}_1 \\ \Delta\dot{W}_1 \\ \dot{e}'_1 \\ \vdots \\ \dot{D}_n \\ \Delta\dot{W}_n \\ \dot{e}'_n \end{bmatrix}$$

$$f(x) = \begin{bmatrix} \Delta\omega_1 \\ -\dfrac{D_1}{2H_1}\Delta\omega_1 - \dfrac{\omega_s}{2H_1}\Delta P_{E1} \\ \tilde{f}_{11} \\ \vdots \\ \Delta\omega_m \\ -\dfrac{D_m}{2H_m}\Delta\omega_m - \dfrac{\omega_s}{2H_m}\Delta P_{Em} \\ \tilde{f}_{1m} \\ \tilde{g}_{11} \\ -\dfrac{D_1}{2H_1}\Delta W_1 - \dfrac{W_s}{2H_1}\Delta P_{e1} \\ \tilde{g}_{21} \\ \vdots \\ \tilde{g}_{1n} \\ -\dfrac{D_n}{2H_n}\Delta W_n - \dfrac{W_s}{2H_n}\Delta P_{en} \\ \tilde{g}_{2n} \end{bmatrix}$$

$$g(x) = \begin{bmatrix} 0 & \cdots & 0 & 0 & \cdots & 0 \\ 0 & \cdots & 0 & 0 & \cdots & 0 \\ 1/T'_{d10} & \cdots & 0 & 0 & \cdots & 0 \\ \vdots & \cdots & \vdots & \vdots & \cdots & \vdots \\ 0 & \cdots & 0 & 0 & \cdots & 0 \\ 0 & \cdots & 0 & 0 & \cdots & 0 \\ 0 & \cdots & 1/T'_{dm0} & 0 & \cdots & 0 \\ 0 & \cdots & 0 & a_{11}/e'_1 & \cdots & 0 \\ 0 & \cdots & 0 & 0 & \cdots & 0 \\ 0 & \cdots & 0 & a_{21} & \cdots & 0 \\ \vdots & \cdots & \vdots & \vdots & \cdots & \vdots \\ 0 & \cdots & 0 & 0 & \cdots & a_{1n}/e'_1 \\ 0 & \cdots & 0 & 0 & \cdots & 0 \\ 0 & \cdots & 0 & 0 & \cdots & a_{2n} \end{bmatrix}$$

$$u = \begin{bmatrix} u_1 \\ \vdots \\ u_m \\ u_{m+1} \\ \vdots \\ u_{m+n} \end{bmatrix} = \begin{bmatrix} u_1 \\ \vdots \\ u_m \\ u_{D1} \\ \vdots \\ u_{Dn} \end{bmatrix}. \tag{7}$$

A first step into implementing the ZD approach is the calculation the system's relative degree. The relative degree of each output $y_i(t) = h_i(x)$ is $r_i, i = 1, \ldots, M$, thus the relative degree of the whole system is $r = r_1 + \cdots + r_M$.

The i-th relative degree of the MIMO system can be calculated by the following conditions:

$$\begin{matrix} L_{\mathrm{g}} L_f^j h_l = 0 \\ L_{\mathrm{g}} L_f^{r_i - 1} h_l \neq 0 \end{matrix}, j < r_i - 1; l = 1, ..., M \tag{8}$$

where, $L_f h_l = \dfrac{\partial h_l}{\partial x} f(x)$ are the Lie derivatives of $h_l(x)$ along $f(x)$ [36].

According to (8), we can easily calculate: $L_{\mathrm{g}_j} h_l = L_{\mathrm{g}_j} L_f^{1-1} h_l = \dfrac{\partial h_i}{\partial X} \mathrm{g}_j(x) \neq 0, l = 1, \ldots, M$, where g_j is the j-th column of matrix $\mathrm{g}(x)$. Therefore, the relative degree of each of the n-SGs and m-DFIGs is equal to one, and the relative degree of the whole system (6) is $r = m + n$ with $r < N$. Hence, the system can be partially linearized using the zero dynamics (ZD) approach.

Define the following nonlinear coordinate transformation:

$$Z = \begin{bmatrix} Z_1 \\ \vdots \\ Z_{r_1} \\ Z_{r_1+1} \\ \vdots \\ Z_{r_1+r_2} \\ \vdots \\ Z_r \\ Z_{r+1} \\ \vdots \\ Z_{r+2m+2n} \end{bmatrix} = \begin{bmatrix} \varphi_{11} \\ \vdots \\ \varphi_{1r_1} \\ \varphi_{2(r_1+1)} \\ \vdots \\ \varphi_{2(r_1+r_2)} \\ \vdots \\ \varphi_{Nr} \\ \eta_1 \\ \vdots \\ \eta_{2m+2n} \end{bmatrix} = \begin{bmatrix} h_1(x) \\ \vdots \\ L_f^{r_1-1} h_1(x) \\ h_2(x) \\ \vdots \\ L_f^{r_2-1} h_2(x) \\ \vdots \\ L_f^{r_N-1} h_N(x) \\ \eta_1 \\ \vdots \\ \eta_{2m+2n} \end{bmatrix}. \tag{9}$$

The most important feature of the ZD approach is its ability to design the control law u such that the outputs of the system $y(t)$ remain equal to zero at $t \geq 0$.

The following conditions should hence be satisfied;

$$\begin{matrix} h_1(x(t)) = h_2(x(t)) = \cdots = h_N(x(t)) = 0 \\ h_l(x(t)) = L_f h_l(x(t)) = \cdots = L_f^{r_l - 1} h_l(x(t)) = 0, \end{matrix} \quad l = 1, ..., N. \tag{10}$$

The Jacobian matrix of (9) can be written as follows:

$$\begin{bmatrix} \dot{Z}_1 \\ \vdots \\ \dot{Z}_m \\ \dot{Z}_{m+1} \\ \vdots \\ \dot{Z}_r \\ \dot{Z}_{r+1} \\ \vdots \\ \dot{Z}_{r+m} \\ \dot{Z}_{r+m+1} \\ \vdots \\ \dot{Z}_{r+2m} \\ \dot{Z}_{r+2m+1} \\ \vdots \\ \dot{Z}_{r+2m+n} \\ \dot{Z}_{r+2m+n+1} \\ \vdots \\ \dot{Z}_{r+2m+2n} \end{bmatrix} = \begin{bmatrix} \dot{h}_1 \\ \vdots \\ \dot{h}_m \\ \dot{h}_{m+1} \\ \vdots \\ \dot{h}_{m+n} \\ \dot{\eta}_1 \\ \vdots \\ \dot{\eta}_m \\ \dot{\eta}_{m+1} \\ \vdots \\ \dot{\eta}_{2m} \\ \dot{\eta}_{2m+1} \\ \vdots \\ \dot{\eta}_{2m+n} \\ \dot{\eta}_{2m+n+1} \\ \vdots \\ \dot{\eta}_{2m+2n} \end{bmatrix} = \begin{bmatrix} v_1 \\ \vdots \\ v_m \\ v_{m+1} \\ \vdots \\ v_{m+n} \\ \Delta\dot{\delta}_1 \\ \vdots \\ \Delta\dot{\delta}_m \\ \Delta\dot{\omega}_1 \\ \vdots \\ \Delta\dot{\omega}_m \\ \Delta\dot{W}_1 \\ \vdots \\ \Delta\dot{W}_n \\ \dot{z}_1 \\ \vdots \\ \dot{z}_n \end{bmatrix}. \tag{11}$$

Based on (10), it can be seen that $\begin{bmatrix} \varphi_{11} & \dots & \varphi_{sr} \end{bmatrix}^T = 0$, which implies $\begin{bmatrix} \dot{\varphi}_{11} & \dots & \dot{\varphi}_{sr} \end{bmatrix}^T = 0$. The control law can be obtained by calculating $v_i = \dot{h}_i,\ i = 1,\dots,m+n$.

Using (3), we can first express $v_i = \Delta\dot{P}_{Ei}, i = 1,\dots,m$ as follows:

$$\begin{aligned} v_i =& \Delta\dot{P}_{Ei} \\ =& \sum_{\substack{j=1 \\ j\neq i}}^{m} \dot{E}'_{qi}E'_{qj}\,\tilde{P}_{1j} + E'_{qi}\left(\dot{E}'_{qj}\,\tilde{P}_{1j} + E'_{qj}\,\Delta\dot{\delta}_i\tilde{Q}_{1j} - E'_{qj}\,\dot{\delta}_j\tilde{Q}_{1j}\right) \\ &+ \sum_{j=1}^{m+n} \dot{E}'_{qi}\,e'_j\,\tilde{P}_{2j} + E'_{qi}\left(\dot{e}'_j\tilde{P}_{2j} + e'_j\,\Delta\dot{\delta}_i\tilde{Q}_{2j} - E'_{qj}\dot{D}_j\tilde{Q}_{2j}\right). \end{aligned} \tag{12}$$

Equation (12) can be re-written as follows:

$$v_i = \Delta\dot{P}_{Ei} = \alpha_{1i} + \alpha_{2i} + \sum_{\substack{j=1 \\ j\neq i}}^{m}\beta_{1j}u_i + \beta_{2j}u_j + \sum_{j=m+1}^{m+n}\beta_{3j}u_i + \beta_{4j}u_{Dj} \tag{13}$$

where the different parameters are defined in the Appendix. Similarly, using (4), we can express $v_k = \Delta\dot{P}_{ek}, k = 1,\dots,n$ as follows:

$$\begin{aligned} v_k =& \Delta\dot{P}_{ek} \\ =& \sum_{j=1}^{m} \dot{e}'_k E'_{qj}\tilde{P}_{3j} + e'_k\left(\dot{E}'_{qj}\tilde{P}_{3j} + E'_{qj}\dot{D}_k\tilde{Q}_{3j} - E'_{qj}\Delta\dot{\delta}_j\tilde{Q}_{3j}\right) \\ &+ \sum_{\substack{j=m+1 \\ j\neq k}}^{m+n} \dot{e}'_k e'_j\tilde{P}_{4j} + e'_k\left(\dot{e}'_j\tilde{P}_{4j} + e'_j\dot{D}_k\tilde{Q}_{4j} - e'_j\dot{D}_j\tilde{Q}_{4j}\right). \end{aligned} \tag{14}$$

Equation (14) can be re-written as follows:

$$v_k = \Delta\dot{P}_{ek} = \alpha_{3k} + \alpha_{4k} + \sum_{j=1}^{m}\beta_{5j}u_j + \beta_{6j}u_{Dk} + \sum_{\substack{j=m+1 \\ j\neq k}}^{m+n}\beta_{7j}u_{Dk} + \beta_{8j}u_{Dj}. \tag{15}$$

Equations (13) and (15) can be re-written in the following format:

$$\begin{bmatrix} v_1 \\ \vdots \\ v_{m+n} \end{bmatrix} = \begin{bmatrix} \Gamma_1 \\ \vdots \\ \Gamma_{m+n} \end{bmatrix} + \begin{bmatrix} W_{11} & \cdots & W_{1(m+n)} \\ \vdots & \ddots & \vdots \\ W_{(m+n)1} & \cdots & W_{(m+n)(m+n)} \end{bmatrix} \begin{bmatrix} u_1 \\ \vdots \\ u_{m+n} \end{bmatrix}. \tag{16}$$

The final control law $\begin{bmatrix} u_1 & \dots & u_{m+n} \end{bmatrix}^T$ can be obtained by solving (22). Thus, for the partially linearized system, all we need to do is design the new control inputs $\begin{bmatrix} v_1 & \dots & v_{m+n} \end{bmatrix}^T$ using a linear control approach [37]. In this paper, the following PI controllers were considered to track the reference:

$$\begin{aligned} v_i &= K_{1i}\Delta P_{Ei} + K_{2i}\int_0^t \Delta P_{Ei}dt,\ \ i = 1,\dots,m \\ v_k &= K_{1k}\Delta P_{ek} + K_{2k}\int_0^t \Delta P_{ek}dt,\ \ k = 1,\dots,n \end{aligned} \tag{17}$$

where the gains K_{1i} and K_{2k} are chosen to minimize the tracking error while ensuring good transient performance.

Note that the zero dynamics approach divides the dynamics of a nonlinear system into two parts: a) the external dynamics, which performance can be achieved through the proper design of a controller.

We need to prove that the zero dynamics of the system are stable. Equations (18)–(25) are given to indicate the internal dynamics are marginal stable. Therefore, the ZD approach is applicable to design coordination controllers of SGs and DFIGs. So, the control law should be selected in such a way that $\lim_{t\to\infty} h_i(x) \to 0$; b) the internal or zero dynamics defined by the last $(M-r)$ rows of the Jacobean matrix $\dot{Z} = \begin{bmatrix} \dot{\varphi} & \dot{\eta} \end{bmatrix}^T$, which should satisfy the following conditions:

$$L_{g_t}\eta_l(x(t)) = 0, l = 1,\dots,M-r; t = 1,\dots,N. \tag{18}$$

Condition (18) is satisfied by selecting:

$$\begin{bmatrix} \dot{Z}_{r+1} \\ \vdots \\ \dot{Z}_{r+m} \\ \dot{Z}_{r+m+1} \\ \vdots \\ \dot{Z}_{r+2m} \\ \dot{Z}_{r+2m+1} \\ \vdots \\ \dot{Z}_{r+2m+n} \\ \dot{Z}_{r+2m+n+1} \\ \vdots \\ \dot{Z}_{r+2m+2n} \end{bmatrix} = \begin{bmatrix} \Delta\dot{\delta}_1 \\ \vdots \\ \Delta\dot{\delta}_m \\ \Delta\dot{\omega}_1 \\ \vdots \\ \Delta\dot{\omega}_m \\ \Delta\dot{W}_1 \\ \vdots \\ \Delta\dot{W}_n \\ \dot{z}_1 \\ \vdots \\ \dot{z}_n \end{bmatrix} \tag{19}$$

where, $z_k, k = 1,\dots,n$ $(r+2m+n+1,\ \dots, r+2m+2n)$ are defined as follows:

$$z_k = \frac{1}{2}\Delta P_{ek}^2 + \frac{1}{2}\Delta W_k^2. \tag{20}$$

Since $\Delta P_{ek} = 0$ at steady state, (20) can be re-written as $\Delta W_{Dk}^2 = 2z_k$. The system dynamics for these states can be expressed as follows:

$$\dot{z}_k = L_f z_k = \Delta W_k \Delta \dot{W}_k. \tag{21}$$

By substituting the fifth equation of (6), $\Delta \dot{W}_k = -\dfrac{D_k}{2H_k}\Delta W_k - \dfrac{W_s}{2H_k}\Delta P_{Ek}$, we can rewrite (21) as follows:

$$\dot{z}_k = L_f z_k = \Delta W_k \left(-\frac{D_k}{2H_k}\Delta W_k - \frac{W_s}{2H_k}\Delta P_{Ek}\right). \tag{22}$$

Since $\Delta P_{ek} = 0$ at steady state

$$\dot{z}_k = -\frac{D_{Dk}}{2H_{Dk}}\Delta W_k^2. \tag{23}$$

Equation (23) can be re-written as follows:

$$\dot{z}_k = -\frac{D_{Dk}}{H_{Dk}} z_k. \tag{24}$$

Equation (24) is a first order differential equation, and we can easily calculate its response as follows:

$$\frac{dz_k}{dt} = -\frac{D_{Dk}}{H_{Dk}} z_k \rightarrow \frac{dz_k}{z_k} = -\frac{D_{Dk}}{H_{Dk}} dt \rightarrow z(t) = Ae^{-\frac{D_{Dk}}{H_{Dk}}}. \tag{25}$$

Therefore, the zero dynamics (internal dynamics) are stable. Equation (24) is the part of zero dynamics of the system, which is stable. The stability of the remaining zero dynamics (internal dynamics) can be proved in the same procedure.

The flowchart of the proposed coordinated approach is depicted in Fig. 1.

The coordinated approach can be summarized as follows:

Step 1: Determine the dynamic equations of the power system as shown in (6).

Step 2: Determine the steady-state point of SG and DFIG using load flow analysis.

Step 3: Calculate the relative degree of the power system by (8), and check the assumption $r < M$.

Step 4: Choose the nonlinear coordinate transformation (9).

Step 5: Check the condition of zero dynamics by (18).

Step 6: Check the stability of zero dynamics.

Step 7: Calculate $\begin{bmatrix} v_1 & \cdots & v_{m+n} \end{bmatrix}^T$ using (13) and (15).

Step 8: Determine PI controllers by (17).

IV. COMPUTER EXPERIMENTS

To illustrate the performance of the proposed coordinated control (Fig. 2), we implemented it to the modified IEEE 39-bus 10-machine New England power system illustrated in Fig. 3 [9].

The New England power system was modified by adding two 200 MW DFIG-based wind turbines at buses 14 and 17, respectively. The parameters of the DFIGs considered in the simulation are listed in Table III in the Appendix. The data used for the SGs, transmission lines and transformers of the power system can be found in [9]. The participation factor method [38] was considered to determine the optimum locations of the excitation controllers of the SGs. The results indicated that the synchronous generators, SG_5, SG_7, and SG_9 are the best locations for designing the excitation controller to damp out the local and inter-areas modes of oscillations. Further, in order to simulate the coupled dynamic response of the wind turbine and prevent the negative interaction between the fast and slow controllers, we implemented the fatigue, aerodynamics, structures, and turbulence (FAST) program proposed by the Renewable Energy Laboratory [39]. Hence, three SGs (m = 3) and two DFIGs (n = 2) were considered in

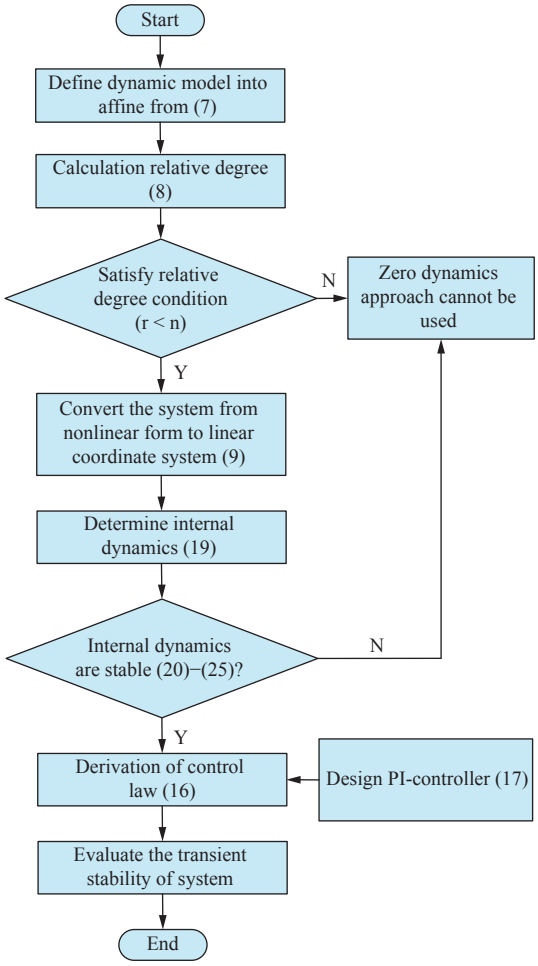

Fig. 1. Flowchart of the proposed coordinated approach.

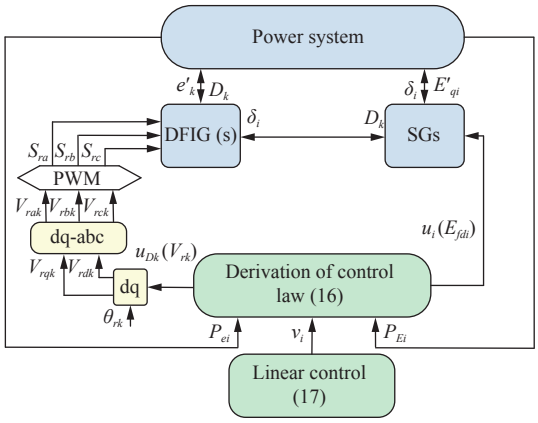

Fig. 2. Block diagram of the proposed approach.

designing the nonlinear coordinated controller. The remaining SGs were equipped with PSS and were not considered in the coordination design implemented in this section. Eigenvalue analysis and time domain simulations were carried out to assess the damping performance and dynamic stability of the proposed approach. The control system dynamics were obtained by solving the differential equations (16) in MATLAB/Simulink environment R2011b version 7.13.

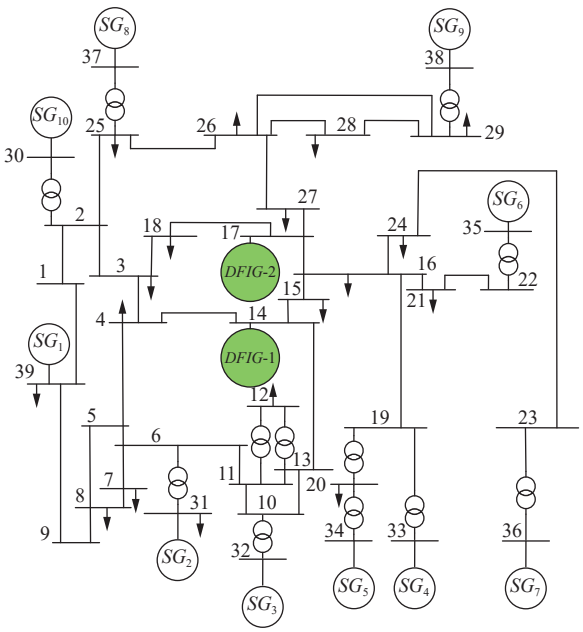

Fig. 3. Single-line diagram of the IEEE 39-bus New England power system.

The performance of the proposed coordinated design was further compared with the following approaches:

1) PSS/POD: the SGs are equipped with power system stabilizers (PSSs), while the DFIGs are equipped with power oscillation dampers (PODs) [9], [40].

2) IDA-PBC: the passivity-based control design method (Interconnection and damping assignment passivity-based control (IDA-PBC)) proposed in [15].

A. Eigenvalues Analysis

Eigenvalue analysis was performed to assess the system's transient performance and damping capabilities. Further, in order to gain insight into the need for a type of control strategy to enhance system's transient dynamics, the eigenvalues were also computed for the case where SGs and DFIGs were not equipped with any controller.

The dominant eigenvalues of the power system at some normal operating conditions are illustrated in Fig. 4 for all the approaches. Note that the minimum damping ratio ($\zeta_{\min}$) of the power system with no controller is 0.0130. The system is clearly undamped and installing a controller for the SGs and DFIGs is a must. Equipping SGs with PSS and DFIGs with POD, however, did slightly improve damping and stabilize the power system. The minimum damping ratio in this case was $\zeta_{\min} = 0.0423$ which means that all system eigenvalues are confined to the conic illustrated in Fig. 4. Implementing the IDA-PBC approach resulted in even better improvement in dominant eigenvalues compared to the PSS/POD ($\zeta_{min} = 0.0830$), but the best results were obtained with the proposed coordinated design ($\zeta_{\min} = 0.1137$) compared to all considered situations. Thus, clearly confirming the ability of the proposed approach to greatly enhance power system damping and transient behavior.

B. Case I: Three-Phase Fault Scenario at Bus 16

In this section, the performance of the proposed approach is evaluated under a three-phase fault condition. This choice is motivated by the fact that such unavoidable fault often results in one of the most severe disturbances to power systems. Assessment was carried over for two scenarios: one that includes DFIGs and one that does not. This aims at evaluating the effectiveness of approach in mitigating the impact of wind energy stems in the grid. Comparison analysis with PSS/POD and IDA-PBC is also carried over. A symmetrical three-phase fault at bus 16 for 100 ms is considered to evaluate the performance of the proposed controller. The rotor angle responses of SG_5, SG_7, and SG_9 with respect to generator SG_{10}, rotor speed and terminal voltage of SG_5, SG_7, and SG_9

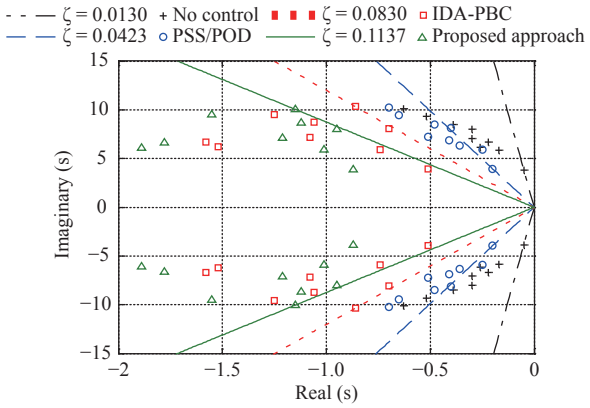

Fig. 4. Dominant eigenvalues for the 39-bus New England system with: (+) no control; (O) PSS/POD; (□) IDA-PBC; (△) the proposed approach.

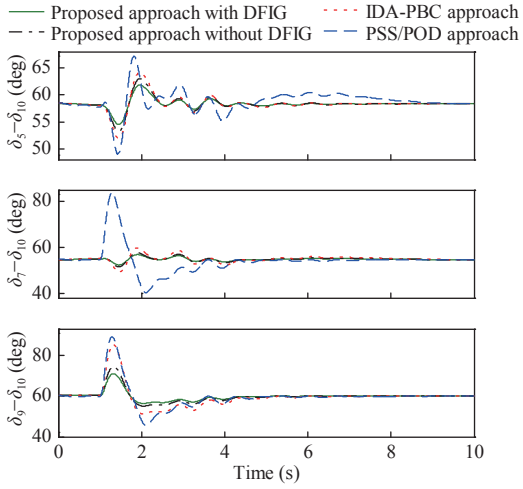

Fig. 5. Rotor angels of SG_5, SG_7, and SG_9 under a three-phase fault at bus 16 (Case I).

generators are illustrated in Figs. 5–7 while the rotor angle responses of $DFIG_1$ and $DFIG_2$ with respect to generator SG_{10} and rotor speed of $DFIG_1$ and $DFIG_2$ are illustrated in Figs. 8 and 9.

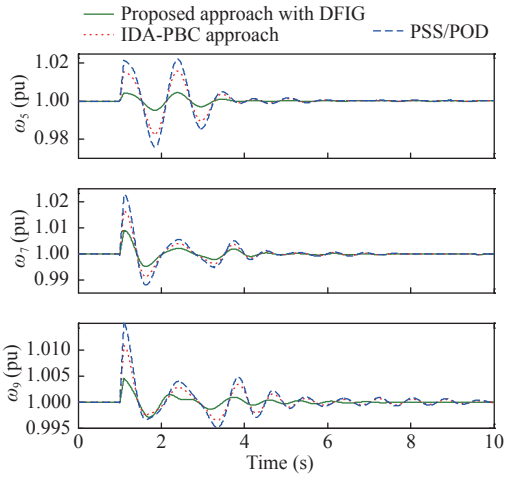

Fig. 6. Rotor speed of SG_5, SG_7, and SG_9 under a three-phase fault at bus 16 (Case I).

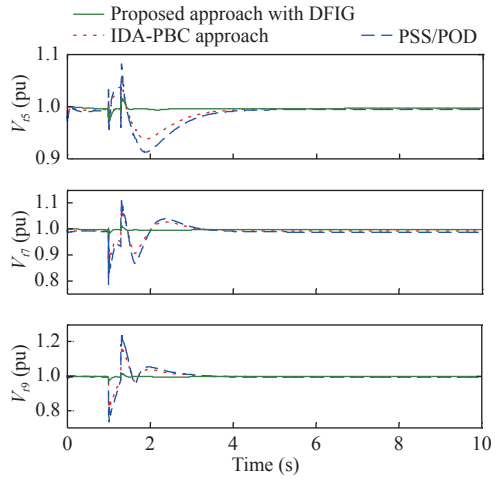

Fig. 7. Terminal voltage of SG_5, SG_7, and SG_9 under a three-phase fault at bus 16 (Case I).

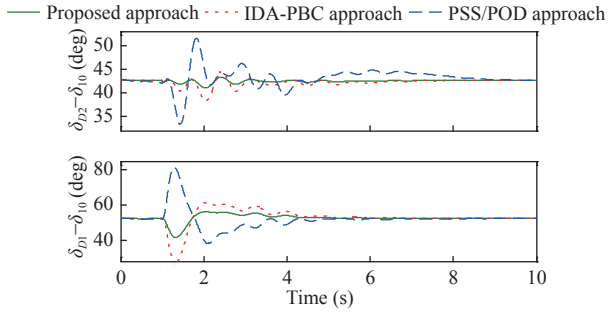

Fig. 8. Rotor angels of $DFIG_1$ and $DFIG_2$ under a three-phase fault at bus 16 (Case I).

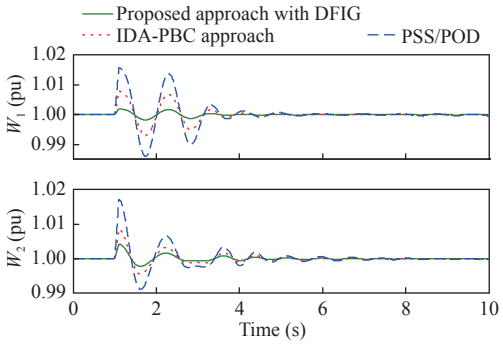

Fig. 9. Rotor speed of $DFIG_1$ and $DFIG_2$ under a three-phase fault at bus 16 (Case I).

Figs. 5–9 show that the post-fault responses of the rotor angles, rotor speed and terminal voltage with PSS/POD and IDA-PBC are quite oscillatory. The time histories of the control signals, E_{fdi} and V_{rk} are depicted in Fig. 10. The range of E_{fdi} and V_{rk} are ∓ 2 pu and ∓ 1.5 pu. Those results confirm that the proposed coordinated approach has significantly improved the power system transient and voltage regulation.

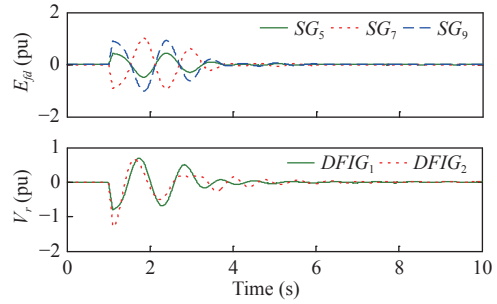

Fig. 10. Control signals of SGs and DFIGs under a three-phase fault at bus 16 (Case I).

The oscillations in the rotor angles were slowly damped however but the rotor took a relatively long time to settle back to their post-fault steady state behavior. Note that, it took the proposed coordinated design less than 2 s from the fault occurrence to damp the oscillations in the rotor angles. Hence, we can conclude that the proposed coordinated approach improves the post-fault transient dynamic response of the system and enables it to regain its steady-state behavior faster than the IDA-PBC method.

C. Case II: Three-Phase Fault Scenario at Bus 34

System performance is assessed in the presence of a symmetrical three-phase fault at the terminal of SG_5 (bus 34). In this case, since the SG will not supply any power when subjected to a three-phase fault at its terminal, the power system may become unstable after the fault is cleared because of the improper damping generated by the excitation system. Further, in order to assess the effectiveness of the proposed approach in dealing with the variability introduced by DFIG-based wind energy systems, the rotor angle of each SG was assessed in the presence and absence of DFIG. The rotor angle responses of SG_5, SG_7, and SG_9 in this case are illustrated in Fig. 11.

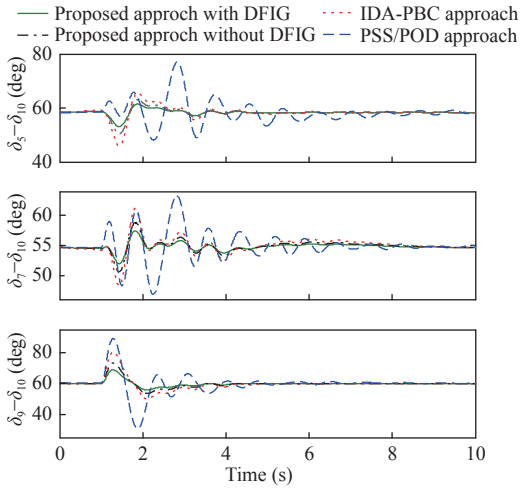

Fig. 11. Rotor angels of SG_5, SG_7, and SG_9 under a three-phase fault at terminal SG_5, bus 34 (Case II).

The results depicted in Fig. 11 show that the proposed approach is able to effectively damp the rotor angle oscillations for power systems with DFIGs. The rotor angle responses of $DFIG_1$ and $DFIG_2$ with respect to generator SG_{10} are illustrated in Fig. 12. Note that, the proposed approach is able to damp the oscillations of the rotor angles faster than the IDA-PBC and PSS/POD approaches.

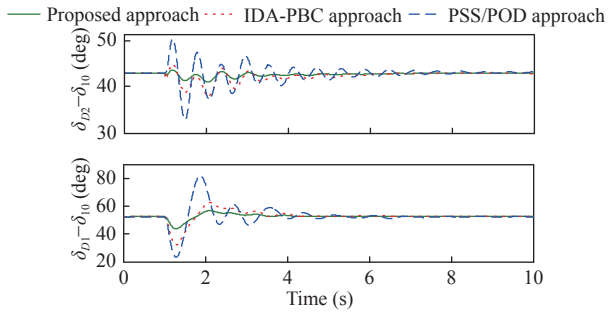

Fig. 12. Rotor angels of $DFIG_1$ and $DFIG_2$ under three-phase fault at terminal SG_5, bus 34 (Case II).

Note that, based on the results depicted in Figs. 11 and 12, both the proposed approach and the IDA-PBC resulted in an enhancement in power system's damping during post-fault operations. However, the proposed coordinated approach performed much better than the IDA-PBC in terms of providing more damping for the torques and faster settling time in achieving the post-fault steady-state operating conditions.

D. Critical Clearing Time (CCT) and Computational Burden analysis

Transient stability refers to the power system's ability to converge to a stable post-fault equilibrium following large disturbances. It is often assessed by how quickly the power system is able to clear a fault so as to maintain the fault-triggered transients inside the stability boundary [32]. Critical clearing time (CCT) is a well-established metric that measures the upper bound of such clearing time. Exceeding this maximum value results in the loss of stability and synchronism by the generators.

In this section, we assess system's transient stability by measuring the CCT following a critical fault such as a three-phase fault occurring at various locations in the power network. The obtained results are illustrated in Table I for the proposed approach, PSS/POD, and IDA-PBC approach.

TABLE I
CRITICAL CLEARING TIME (CCT) OF THE DIFFERENT APPROACHES

Fault location	Approaches	CCT (ms)	CCT improvement compared to PSS/POD (%)
Bus 34	PSS/POD	140	
	IDA-PBC	150	7.14%
	Proposed approach	170	21.42%
Bus 16	PSS/POD	150	
	IDA-PBC	165	10.00%
	Proposed approach	185	23.33%
Bus 26	PSS/POD	170	
	IDA-PBC	185	8.82%
	Proposed approach	200	17.64%

Table I shows that the proposed coordinated control approach resulted in an improvement of critical clearing time and subsequently transient stability by up to 23.33% for the considered fault.

Further, the three approaches were qualitatively compared in terms of mathematical complexity, computational cost, reliability and robustness. The comparison analysis is illustrated in Table II.

TABLE II
COMPUTATIONAL BURDEN AND VARIOUS PARAMETERS OF THE DIFFERENT APPROACHES

Computational parameters	**Proposed approach**	**IDA-PBC**	**POD/PSS**
Robustness level	Too high	High	Low
System stability	Too high	High	Low
Mathematical complexity	High	Too high	Low
System linearization	Partial	Full	None
Reliability	High	High	Low
Self-tuning capability	High	Low	None
Computational cost	High	Too high	Low
Settling time	Too fast	Fast	Slow

Note that, though the mathematical complexity and computational cost of the proposed approach is higher than that of the traditional PSS/POD, it outperforms this latter in terms of stability, robustness, transient performance, and application to large scale power systems. The computational burden and mathematical complexity of the proposed approach is lower than that of the IDA-PBC approach however.

Based on the above results and discussions, we can conclude that the proposed coordinated design enhances the

transient stability and performance of large scale power systems with SGs and DFIG-based wind energy systems, while keeping a reasonable computational cost.

V. Conclusion

This paper proposed a coordinated framework for large scale power systems with DFIG-based wind turbines and synchronous generators (SGs). The design is based on the multi input-multi output (MIMO) zero dynamics (ZD) approach and aims at enhancing power system's transient stability. It captures system's nonlinearities and considers the dynamic interactions among the various generators. The proposed framework resulted in faster post-fault recovery time and better transient stability compared to other approaches such as PSS/POD and IDA-PBC. One of the main features of the proposed approach is its ability to reduce the order of the feedback linearized power system, thus making the coordinated control design simple and cost effective. Further, the proposed approach can easily be implemented, in practice, using synchronized phasor measurement units (PMUs). These latter can be installed on the bus of each generator to estimate all the parameters of the network and generators needed for small signal stability analysis.

In closing, we recognize that the multi-machine power system results presented in this paper are preliminary and that there is considerable work that needs to be done to extend this approach to large-scale power systems with different types of renewable energy sources such as PV systems, and/or considering delay time of the controllers [41]. However, we have clearly shown that integrating a DFIG into power systems using a nonlinear coordinated control design methodology has the potential to improve power system performance. We are currently working to demonstrate these results on the laboratory scale power system.

APPENDIX

$$\tilde{P}_{1j}=B_{ij}\sin\delta_{ij},\tilde{P}_{2j}=B_{ij}\sin\left(\delta_i-D_j\right)$$

$$\tilde{P}_{3j}=B_{ij}\sin\left(D_i-\delta_j\right),\tilde{P}_{4j}=B_{ij}\sin D_{ij}$$

$$\tilde{Q}_{1j}=B_{ij}\cos\delta_{ij},\tilde{Q}_{2j}=B_{ij}\cos\left(\delta_i-D_j\right)$$

$$\tilde{Q}_{3j}=B_{ij}\cos\left(D_i-\delta_j\right),\tilde{Q}_{4j}=B_{ij}\cos D_{ij}$$

$$\alpha_{1i}=\sum_{\substack{j=1\\ j\neq i}}^{m}E'_{qi}\left(E'_{qj}\Delta\dot{\delta}_i\tilde{Q}_{1j}-E'_{qj}\Delta\dot{\delta}_j\tilde{Q}_{1j}\right)+\tilde{P}_{1j}\left(\tilde{f}_{1i}E'_{qj}+\tilde{f}_{1j}E'_{qi}\right)$$

$$\alpha_{2i}=\sum_{j=m+1}^{m+n}e'_j\tilde{P}_{2j}\tilde{f}_{1i}+E'_{qi}e'_j\Delta\dot{\delta}_i\tilde{Q}_{2j}+E'_{qi}\left(\tilde{g}_{2j}\tilde{P}_{2j}-e'_j\tilde{g}_{1j}\tilde{Q}_{2j}\right)$$

$$\alpha_{3i}=e'_k\sum_{j=1}^{m}E'_{qj}\tilde{Q}_{3j}\left(\tilde{g}_{1k}-\Delta\dot{\delta}_j\right)+\sum_{j=1}^{m}\tilde{P}_{3j}\left(\tilde{g}_{2k}E'_{qj}+\tilde{f}_{1j}e'_k\right)$$

$$\alpha_{4i}=\sum_{\substack{j=m+1\\ j\neq k}}^{m+n}\tilde{P}_{4j}\left(\tilde{g}_{2k}e'_j+\tilde{g}_{2j}e'_k\right)+e'_k\left(e'_j\tilde{Q}_{4j}\left(\tilde{g}_{1k}-\tilde{g}_{1j}\right)\right)$$

$$\beta_{1j}=\frac{\tilde{P}_{1j}E'_{qj}}{T'_{di0}}$$

$$\beta_{2j}=\tilde{P}_{1j}E'_{qi}/T'_{dj0}$$

$$\beta_{3j}=e'_j\tilde{P}_{2j}\tilde{f}_{1i}/T'_{di0}$$

$$\beta_{4j}=E'_{qi}\left(a_{2j}\tilde{P}_{2j}-a_{1j}\tilde{Q}_{2j}\right)$$

$$\beta_{5j}=\frac{\tilde{P}_{3j}e'_k}{T'_{dj0}}$$

$$\beta_{6j}=a_{2k}\tilde{P}_{3j}E'_{qj}+E'_{qj}\tilde{Q}_{3j}a_{1k}$$

$$\beta_{7j}=e'_j\left(a_{2k}\tilde{P}_{4j}+a_{1k}\tilde{Q}_{4j}\right)$$

$$\beta_{8j}=e'_k\left(a_{2j}\tilde{P}_{4j}-a_{2j}\tilde{Q}_{4j}\right).$$

TABLE III
DFIG Parameters

Parameter	Value
Nominal power/Voltage/Frequency	200 (MW)/575 (V)/60 (Hz)
Number of pole pairs	3
R_s	0.007060 (pu)
L_s	0.1710 (pu)
M	2.9000 (pu)
R_r/L_r	0.0050 (pu)/0.156 (pu)
R_g/L_g	0.19838 (mΩ)/ 0.052621 (mH)

References

[1] M. J. Morshed, A. Fekih, "A novel fault ride through scheme for hybrid wind/PV power generation systems," *IEEE Trans. Sustainable Energy*, pp. 1–10, 2019. DOI: 10.1109/TSTE.2019.2958918.

[2] R. Mathe and K. Folly, "Impact of large scale grid-connected wind generators on the power system network," in *Proc. IEEE PES Power Africa*, pp. 328–333, Jul. 2017.

[3] M. J. Morshed and A. Fekih, "A fault-tolerant control paradigm for microgrid-connected wind energy systems," *IEEE Syst. J.*, vol. 12, no. 1, pp. 360–372, 2018.

[4] J. Stoolmeg and W. Kling, "The impact of large scale wind power generation on power system oscillations," *Electric Power Systems Research*, vol. 67, no. 1, pp. 9–20, 2003.

[5] M. J. Morshed and A. Fekih, "A probabilistic robust coordinated approach to stabilize power oscillations in DFIG-based power systems," *IEEE Trans. Ind. Informatics*, vol. 15, no. 10, pp. 5599–5612, 2019.

[6] Y. Mishra, S. Mishra, M. Tripathy, N. Senroy, and Z. Y. Dong, "Improving stability of a DFIG-based wind power system with tuned damping controller," *IEEE Trans. Energy Convers.*, vol. 24, no. 3, pp. 650–660, Sept. 2009.

[7] A. Rahim and I. Habiballah, "DFIG rotor voltage control for system dynamic performance enhancement," *Electr. Power Syst. Res.*, vol. 81, no. 2, pp. 503–509, Feb. 2011.

[8] J. Taft, P. De Martini, and R. Geiger, " Ultra large scale power system control and coordination architecture. A strategic framework for

integrating grid functionality," Report preapared by Pacific Northwest National Lab. for the US Department of Energy, Jun. 2014.

[9] T. Surinkaew and I. Ngamroo, "Coordinated robust control of DFIG wind turbine and PSS for stabilization of power oscillations considering system uncertainties," *IEEE Trans. Sustain. Energy*, vol. 5, no. 3, pp. 823–833, Jul. 2014.

[10] Y. Liu, Q. Wu, and X. Zhu, "Coordinated switching controllers for transient stability of multi-machine power systems," *IEEE Trans. Power Syst.*, vol. 31, no. 5, pp. 3937–3949, Sept. 2016.

[11] J. Chen, R. Huang, J. Zhang, and Z. Lin, "Decentralized adaptive controller design for large scale power systems" in *Proc. Chinese Automation Congr.*, pp. 1377–1382, 2015.

[12] A. Okou, L. Dessaint, and O. Akhrif, "Globally stabilizing robust adaptive voltage and speed regulator for large-scale power systems," in *Proc. IEEE Conf. Decision and Control*, pp. 6472–6479, 2005.

[13] C. King, J. Chapman, and M. Ilie, "Feedback linearizing excitation control on a full-scale power system model," *IEEE Trans. Power Syst.*, vol. 9, no. 2, pp. 1102–1109, May 1994.

[14] A. Leon, J. Solsona, and M. Valla, "Comparison among nonlinear excitation control strategies used for damping power system oscillations," *Energy Conver. Management*, vol. 53, no. 1, pp. 55–67, 2012.

[15] A. Kanchanaharuthai, V. Chankong, and K. A. Loparo, "Transient stability and voltage regulation in multimachine power systems Vis-à-Vis STATCOM and battery energy storage," *IEEE Trans. Power Syst.*, vol. 30, no. 5, pp. 2404–2416, Sept. 2015.

[16] M. Mahmud, M. Hossain, H. Pota, and M. Amanullah, "Robust partial feedback linearizing excitation controller design for multimachine power systems," *IEEE Trans. Power Syst.*, vol. 32, no. 1, pp. 3–16, 2017.

[17] T. Orchi, T. Roy, M. Mahmud, and A. Too, "Feedback linearizing model predictive excitation controller design for multimachine power systems," *IEEE Access*, vol. 6, pp. 2310–2319, Feb. 2018.

[18] A. Isidori, "Nonlinear zero dynamics," in *Encyclopedia of Systems and Control*, Springer-Verlag, 2014.

[19] G. Kenne, J. D. N. Ndongmo, R. F. Kuate, and H. B. Fotsin, "An online simplified nonlinear controller for transient stabilization enhancement of DFIG in multi-machine power systems," *IEEE Trans. Automatic Control*, vol. 60, no. 9, pp. 2664–2669, Sept. 2015.

[20] H. Yassami, F. Bayat, A. Jalilvand, and A. Rabiee, "Coordinated voltage control of wind-penetrated power systems via state feedback control," *Int J. Elect Power Energy Syst.*, vol. 93, pp. 384–394, 2017.

[21] F. Wu, X. Zhang, P. Ju, and M. J. H. Sterling, "Decentralized nonlinear control of wind turbine with doubly fed induction generator," *IEEE Trans. Power Syst.*, vol. 23, no. 2, pp. 613–621, 2008.

[22] M. Edrah, K. L. Lo, and O. Anaya-Lara, "Impacts of high penetration of DFIG wind turbines on rotor angle stability of power systems," *IEEE Trans. Sustainable Energy*, vol. 6, no. 3, pp. 759–766, 2016.

[23] M. J. Morshed, Z. Sardoueinasab, and A. Fekih, "A coordinated control for voltage and transient stability of multi-machine power grids relying on wind energy," *Int. J. Electrical Power Energy Syts.*, vol. 109, pp. 95–109, 2019.

[24] H. Mahvash, S. A. Taher, M. Rahimi, and M. Shahidehpour, "DFIG performance improvement in grid connected mode by using fractional order [PI] controller," *Int J. Elect Power Energy Syst.*, vol. 96, pp. 398–411, 2018.

[25] O. J. K. Oghorada and L. Zhang, "Analysis of star and delta connected modular multilevel cascaded converter-based STATCOM for load unbalanced compensation," *Int J. Elect. Power and Energy Syst.*, vol. 95, pp. 341–352, 2108.

[26] W. Li and T. Dinh-Nhon, "Stability enhancement of DFIG-based offshore wind farm fed to a multi-machine system using a STATCOM," *IEEE Trans. Power Syst.*, vol. 28, no. 3, pp. 2882–2889, 2013.

[27] Y. Lu, *Electric Power System Dynamics*. London: Academic, 1983.

[28] P. Kundur, *Power System Stability and Control*. New York, NY, USA: McGraw-Hill, 1994.

[29] M. Shakarami and I. Davoudkhani, "Wide-area power system stabilizer design based on grey wolf optimization algorithm considering the time delay," *Electric Power Syst. Res.*, vol. 133, pp. 149–159, 2016.

[30] K. Elkington and M. Ghandari, "Comparison of reduced order doubly fed induction generator models for nonlinear analysis," in *Proc. IEEE Electrical Power & Energy Conf.*, pp. 1–6, 2009.

[31] Y. Shang, "Resilient consensus of switched multi-agent systems," *Systems & Control Letters*, vol. 122, pp. 12–18, Dec. 2018.

[32] M. J. Morshed, Z. Sardoueinasab, and A. Fekih, "A nonlinear coordinated approach to enhance the transient stability of wind energy-based power systems," in *Proc. 58th IEEE Conf. Decision and Control*, pp. 6560–6565, 2019.

[33] J. Chiasson, *Modeling and High-Performance Control of Electric Machines*. New York: Wiley, 2005.

[34] A. Khodabakhshian, M. J. Morshed, and M. Parastegari, "Coordinated design of STATCOM and excitation system controllers for multi-machine power systems using zero dynamics method," *Int. J. Elect. Power Energy Syst.*, vol. 49, pp. 269–279, 2013.

[35] G. Kenne, R. Gomac, H. Nkwawob, F. Lamnabhi-Lagarrigue, A. Arzande, and J. C. Vannier, "An improved direct feedback linearization technique for transient stability enhancement and voltage regulation of power generators," *Int. J. Electrical Power and Energy Syst.*, vol. 32, pp. 809–816, 2010.

[36] A. Isidori, *Nonlinear Control Systems*. Springer: London, 1995.

[37] M. Chowdhury, M. Mahmud, W. Shen, and H. Pota, "Nonlinear controller design for series-compensated DFIG-based wind farms to mitigate subsynchronous control interaction," *IEEE Trans. Energy Conv.*, vol. 32, no. 2, pp. 707–719, Jun. 2017.

[38] Y. Tang, J. Zhong, and J. Liu, "A generation adjustment methodology considering fluctuations of loads and renewable energy sources," *IEEE Trans. Power Sys.*, vol. 31, no. 1, pp. 125–132, Jan. 2016.

[39] M. Singh, E. Muljadi, J. Jonkman, V. Gevorgian, I. Girsang, and J. Dhupia, "Simulation for wind turbine generators-with FAST and MATLAB-simulink modules," National Renewable Energy Lab., Report, 2014.

[40] H. Huang, C. Chung, "Coordinated damping control design for DFIG-based wind generation considering power output variation," *IEEE Trans. Power Syst.*, vol. 27, no. 4, pp. 1916–1925, Nov. 2012.

[41] Y. Shang, "On the delayed scaled consensus problems," *Appl. Sci.*, vol. 7, pp. 2–10, 2017.

Mohammad Javad Morshed (S' 14–M' 18) received the M.S. degree from the University of Isfahan, Iran, in 2011, and the Ph. D. degree from the University of Louisiana at Lafayette, USA, both in electrical engineering. His research interests include nonlinear and robust control, optimal control, fault tolerant control with applications to power systems, power systems stability and control, FACTS devices, power electronics, and renewable energy grid integration.